KSME

Springer

Journal of Mechanical Science and Technology 35 (9) 2021

Original Article
DOI 10.1007/s12206-021-0803-x

Keywords:
· FEM
· FGM
· SMP
· SMPC
· VIL

Correspondence to:
Kanif Markad
kmarkad13@gmail.com

Citation:
Lal, A., Markad, K. (2021). Static and dynamic nonlinear stability analyses of hybrid sandwich composite beams under variable in-plane loads. Journal of Mechanical Science and Technology 35 (9) (2021) 3895~3908.
http://doi.org/10.1007/s12206-021-0803-x

Received February 17th, 2021
Revised May 12th, 2021
Accepted May 23rd, 2021

† Recommended by Editor
No-cheol Park

Static and dynamic nonlinear stability analyses of hybrid sandwich composite beams under variable in-plane loads

Achchhe Lal and Kanif Markad

Mechanical Engineering Department, SVNIT, Surat-395007 (GJ), India

Abstract Post-buckling and dynamic nonlinear stability analyses of a sandwich functionally graded material (FGM) composite beam subject to in-plane compressive static and periodic loading are conducted by implementing a higher-order shear deformation with von Karman kinematics. The dynamic instability region is evaluated using the Mathieu-Hill-type equation in Bolotin's method. Comparisons of the layered composite beam, FGM sandwich composite beam, shape memory polymer (SMP) composite beam, and SMP-FGM sandwich composite beam with variable in-plane loads (N_x^1, N_x^2, N_x^3) are depicted for the first time in the current work. The unstable region of N_x^3 is lower compared with those of N_x^1 and N_x^2.

1. Introduction

Composite laminated panels perform well when the weights of structures are reduced, but a sudden sideway deflection may occur due to the application of in-plane compressive loads [1, 2]. Thus, the stability response of structures under in-plane loads should be studied as a means of exploring the possibility of safe and efficient structures, which may find their applications in robotics, naval, aerospace, automobile, electronics, civil, and many more industries [3]. The literature about linear and nonlinear buckling and post-buckling analysis of composite beams is extensive. For instance, Akbas [4] studied the composite beam and its hygrothermal effect via post-buckling analysis with respect to first-order shear deformation theory (FSDT) and the finite element method (FEM). Song et al. [5] and Lee et al. [6] utilized higher-order theory with the cubic dispersal of the displacement field equation and classical laminate theory to analyze thin-walled composite beams. Singh and Chakrabarti [7] utilized zigzag theory (with higher-order configuration) with C^o continuity to predict the buckling response of laminated composite structures. Whenever structures undergo a temperature variation either due to environmental conditions or working conditions, their stability will be affected.

Intelligent/smart materials are engineered materials that are sensitive to one or more stimuli, such as voltage, pH, pressure, temperature, and magnetism, and their electric current can be significantly altered and controlled by internal molecular bonds [8, 9]. Shape memory polymers (SMPs) are stimulated by temperature and have an outstanding shape memory property with appreciable shape recovery and fixity; however, with prolonged usage, a thermal depreciation occurs, resulting in the decline of the mechanical properties of these polymers [10]. Thus, to gain the advantage of superior shape memory property of SMPs, researchers have developed shape memory polymer composites (SMPCs) by reinforcing fibers or particles into SMPs [11]. Zhang et al. [12] and Lal and Markad [13] assessed the behavior of SMPs and analyzed the corresponding SMPC behavior via bending analysis either by analytical modeling, such as based on Euler–Bernoulli beam theory (with or without FEM), or experimentally in the vicinity of glass transition temperature (T_g). Extensive research is available regarding the buckling and vibrational analyses of composite materials and structures, but the work for SMPs and their corresponding smart composites are inadequate. Moreover, the literature hardly discusses the post-buckling and dynamic responses of SMP sandwich composite structures.

Maintaining structural integrity and the expected performance under critical loading conditions and drastic temperature variation is one of the prime objectives of structural engineers who deal with skyscrapers or space habitats. In view of contributing to this direction, researchers have analyzed the static and dynamic stability of isotropic and composite structures. Zizicas [14] studied dynamic stability for the dynamic buckling of thin plates with respect to time-dependent loads. Subsequently, a comprehensive research on the dynamic stability was conducted for isotropic and composite structures, some of which were by Librescu and Chandiramani [15] and Ozturk and Sabuncu [16]. Touratier [17] and Beakou and Touratier [18] utilized C^1 eight-node shear-flexible plate elements. The dynamic stability analysis of a cantilever composite beam was performed by Loja et al. [19] and Binnur [20] for potential applications in aircraft, helicopter and naval propeller, and blades of turbines under in-plane loads. Ozturk and Sabuncu [16] and Karaagac et al. [21] performed a stability analysis of specimens under periodic in-plane loading by using FEM with different slenderness ratios, ply orientations, and springs with torsional supports.

Functionally graded materials (FGMs) can be gradually varied according to their structural and composition properties to influence the volume of these materials, thus further improving their properties. FGMs can improve the resistance of polymer composites when they are thermally degraded at elevated temperatures. On the basis of third-order shear deformation plate theory (TSDT), Thanh et al. [22] analyzed the nonlinear dynamic responses by applying dynamic loads onto functionally graded (FG)-single-walled nanotube-reinforced composite (SWCNTRC) elastic foundation plates. Fu et al. [23] and Duc et al. [24] studied thermo-piezoelectric FGM panels with Euler–Bernoulli beam and higher-order shear deformation (HSDT) plate theory and determined their dynamic stability response via buckling and free vibrational analyses to predict the effect of thermo-electro-mechanical and electric properties on thermal loads. Shen [25, 26] examined FGM plates and inferred the absence of classical bifurcation buckling under thermal environments via the perturbation method. Fazzolari [27] investigated the critical buckling load (CBL) of laminated composite plates containing FGM by considering the hierarchical trigonometric Ritz formulation. Zamanzadeh et al. [28] and Trinh et al. [29] performed static and dynamic nonlinear analyses of FG microbeams by improving the couple stress concept for buckling and vibration mode shapes. Duc et al. [30-32] presented the response of FGM and FG-SWCNTRC circular cylindrical shells subject to thermo-electro-mechanical, damping, and uniformly distributed dynamic loads in thermal environments. Duc and Pham [33] presented the response of FG-SWCNTRC truncated conical shells resting on elastic foundations subject to dynamic loads based on classical shell theory. In an extension work, Duc et al. [34-39] investigated the nonlinear dynamic responses of the FG-SWCNTRC double-curved shallow shell panel and auxetic honeycomb core by using FSDT, TSDT, and HSDT together with classical shell theory.

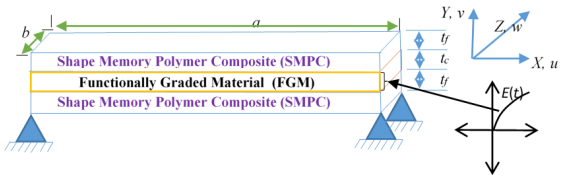

Fig. 1. Geometry of the SMPFGMSC beam.

According to the review of literature, the static and dynamic analyses of laminated composite structures and FGM beams have been sufficient. By contrast, the static buckling analysis of SMPC laminates with FGM has not been comprehensively explored. Current studies have also revealed the insufficient dynamic stability and instability analyses of SMPCs with FGM beams with different beam parameters, boundary conditions (BCs), and temperatures.

In the present study, on the basis of HSDT with FEM and von Karman nonlinearity, a critical buckling analysis of the SMPC sandwich FGM composite beam is conducted. The dynamic instability region is evaluated by using the Mathieu–Hill-type equation in Bolotin's method. Furthermore, the effect of temperature and amplitude ratio variation on FGM beams is determined for the first time along with the clear differentiation among layered, sandwich, FGM, and sandwich FGM composite beams. The comparative results among layered composites, FGM sandwich composites, SMPCs, and SMPFGMSCs with different variable in-plane loads (VILs) are also depicted for first time in the current work.

2. Geometrical configuration of the composite beam

The present analysis focuses on the SMPFGMSC beam, as shown in Fig. 1. The dimensions and the coordinate system are analyzed. The facesheet and bottom sheet of the sandwich composite are made of SMPC, and the core is an FGM. This FGM is composed of metal and ceramic constituents. Its composition varies with thickness, i.e., z = h/2 for a ceramic-rich FGM beam and z = −h/2 for a metal-rich FGM beam.

In the analysis, attention is given to the shape memory polymer functionally graded material sandwich composite (SMPFGMSC) beam with dynamic temperature and dynamic load variations. In this manner, the beam's instability and buckling behavior can be determined.

The beam properties of the FGM are varied, such as the thickness, as denoted by the power low index [29].

$$L(z) = V_k\left(L_C - L_m\right) + L_m \tag{1}$$

where the ceramic and metal constituent properties are defined by the superscripts c and m, respectively, and V_k is the volume fraction of the material (k) along z and defined as $\left[\left(z/h\right)+\left(1/2\right)\right]^n$, where n is the volume fraction exponent. If the temperature-dependent (TD) properties are considered,

Table 1. Comparison of CBLs for various BCs.

Lamina stacking	CF			CC		
	Ozturk [16]	Reddy [48]	Present	Ozturk [16]	Reddy [48]	Present
0	5.14	5.14	5.31	82.25	82.24	81.54
90	0.21	0.20	0.20	3.29	3.29	3.48
[0/90]s	4.51	4.53	4.43	72.10	72.50	71.32
[90/0]s	0.79	0.82	0.82	12.77	13.18	14.00
	[2] Quasi 3D	[2] HBT	Present	[2] Quasi 3D	[2] HBT	Present
[0/C/0]	4.17	3.59	3.65	5.51	6.15	6.57
[0/90/0]	3.36	3.39	3.22	5.11	5.39	5.98
[0/90]	1.25	1.26	1.36	4.347	4.57	4.20

then the effective material parameters can be written as $M = M_0\left[\left(\frac{M_{-1}}{T}\right)+1+M_1T+M_2T^2+M_3T^3\right]$, where M_i(i = -1, 0, 1, 2, 3) represent the temperature coefficients whose values are taken from the study of Trinh et al. [29]. The details are listed in Table 1.

2.1 Evaluation of properties of SMPC sheets

According to the reviewed literature, previous researchers had evaluated the material properties of SMP matrices via experimentation techniques (e.g., Westbrook et al. [40]) and the optimization method (e.g., Gu et al. [41, 42]). Mahieux [43] presented the method of estimation storage modulus of SMPs in the vicinity of glass transition temperature (T_g), which is given by

$$E_m = \left(E_1 - E_2\right)e^{\left(-(X_2)^{m_1}\right)} + (E_2 - E_3)e^{\left(-(X_4)^{m_2}\right)} + E_3\exp\left(-(X_5)^{m_3}\right), \quad (2)$$

were $X_2 = T/T_\beta$, $X_4 = T/T_g$, and $X_5 = T/T_f$, and T is the temperature variation in the analysis. At certain temperatures, the β transition ($T_\beta = 295.2$ K), flow region ($T_f = 415.5$ K), glass transition ($T_g = 305$ K), and the elastic moduli of the SMP are $E_1 = 2.552$ Gpa, $E_2 = 1.876$ Gpa, and $E_3 = 5$ Mpa. The Weibull exponents are represented as $m_1 = 19.3$, $m_2 = 58.4$, and $m_3 = 177.6$ in the equation. The values of all of the abovementioned constants are taken from Gu et al. [41]. The validation of the storage modulus variation with temperature is shown in Fig. 8. In the figure, E_m is the elastic modulus of the polymer in the analysis. Similar to E_m, the Poisson's ratio is evaluated on the basis of the phase transition model for SMP materials as follows [44]:

$$\mu = \mu_g v_g + \mu_r\left(1 - v_g\right), \quad (3)$$

$$v_g = 1 - X_6,\ X_6 = 1/1+\exp\left[-\left(T - T_m\right)/Z\right]. \quad (4)$$

The reference temperature is denoted by $T_m = 300.5$ K, $\mu_g = 0.35$, and $\mu_r = 0.499$. The phase transition zone width is defined as $Z = 7$. According to Eqs. (2)-(4), the effective material properties of the SMP can be obtained and then used in the evaluation of the properties of the SMPC with carbon fiber reinforcement. The properties of the carbon fiber in this study are $E_{1f} = 230$ Gpa, $E_{2f} = 8.2$ Gpa, $G_{12f} = 27.3$ Gpa, $\mu_f = 0.25$, $\alpha_{1f} = -8.3\times10^{-7}$ /°C, $\alpha_{2f} = 10\times10^{-6}$ /°C, and C = 0.2. According to Qi et al. [44] and Lal and Markad [13], the effective material properties of the transversely isotropic SMPC can be evaluated using the volume averaging method as follows:

$$E_{s1} = \upsilon_m E_m + \upsilon_f E_{1f}, \quad (5a)$$

$$E_{s2} = \left(1 - S\right)E_{s2}^1 + SE_{s2}^2, \quad (5b)$$

$$\mu_{s21} = \left(1 - S\right)\mu_{s21}^1 + S\mu_{s21}^2, \quad (5c)$$

$$\mu_{s12} = \mu_{s21}\left(E_{s2}/E_{s1}\right), \quad (5d)$$

$$G_{s12} = \left(1 - S\right)G_{s12}^1 + SG_{s12}^2. \quad (5e)$$

In Eqs. (5a)-(5e), the values of the unknowns are defined as follows:

$$E_{s2}^1 = \left(E_m E_{2f}\right)/\left(\upsilon_f E_m + \upsilon_m E_{2f}\right);\ E_{s2}^2 = \upsilon_m E_m + \upsilon_f E_{2f};$$
$$\mu_{s21}^1 = \upsilon_m \mu_m + \upsilon_f \mu_f;$$
$$\mu_{s21}^2 = \left(\mu_f \upsilon_m E_{2f} + \mu_m E_m \upsilon_m\right)/\left(\upsilon_f E_{2f} + \upsilon_m E_m\right);$$
$$G_{s12}^1 = \left(G_{12f} G_m\right)/\left(\upsilon_m G_{12f} + G_m \upsilon_f\right);\ G_{s12}^2 = \upsilon_f G_{12f} + G_m \upsilon_m.$$

2.2 Displacement field equation

When analyzing the nature of the behavior of any arbitrary point within a sandwich composite beam along the x and z directions, the modified generalized equation can be written as follows [13, 45]:

$$U = u_x + z\varphi_x - \left(4/3h^2\right)z^3\varphi_x - \left(4/3h^2\right)z^3\left(\partial w/\partial x\right) \text{ and } W = w_x \quad (6)$$

where the mid-plane displacements in the x and z directions are represented by u and w, respectively, and the slope and rotation in the x direction are denoted by $\left(\varnothing_x = \frac{\partial w}{\partial x}\right)$ and φ_x, respectively. Four DOFs are utilized in the present analysis, and the displacement vector represented as follows [46]:

$$\{p\} = \{u\ w\ \varnothing_x\ \varphi_x\}. \quad (7)$$

2.3 Relation of displacement, stress, and strain

According to basis of large deformation theory that considers

von Karman nonlinearity, the relation between stress and strain for the plane stress case can be written as

$$\bar{\sigma} = \begin{bmatrix} Q_{11} & 0 \\ 0 & Q_{55} \end{bmatrix} [T]\{\bar{\varepsilon}_l\} + \begin{bmatrix} Q_{11} & 0 \\ 0 & Q_{55} \end{bmatrix} \frac{1}{2} [A_{nl}]\{\phi_{nl}\}. \quad (8)$$

Eq. (8) contains the step vector [*T*] and the $\{\bar{\varepsilon}_l\}$ linear. The strain tensor is defined as

$$[T] = \begin{bmatrix} 1 & z & z^3 & 0 & 0 \\ 0 & 0 & 0 & 1 & z^2 \end{bmatrix}, \{\bar{\varepsilon}_l\} = [B]\{q\}.$$

2.4 Strain energy of the SMPFGMSC beam

The capacity of the forces (internal) or stresses to manifest deformation or strain in the beam is assumed as the strain energy of that beam. The strain energy of the sandwich SMPFGMSC beam represents the combination of the linear and nonlinear strain energies of the beam. The total strain energy (S_T) given in Eq. (10).

$$S_T = S_l + S_{nl}. \quad (9)$$

The linear and nonlinear strain energies are expressed as

$$S_T = 1/2 \int_A [\{\bar{\varepsilon}_l\}^T [D]\{\bar{\varepsilon}_l\} dA] + [\{\bar{\varepsilon}_l\}[D_1]\{\bar{\varepsilon}_{nl}\}^T + \{\bar{\varepsilon}_{nl}\}[D_2]\{\bar{\varepsilon}_l\}^T + \{\bar{\varepsilon}_{nl}\}[D_3]\{\bar{\varepsilon}_{nl}\}^T] dA. \quad (10)$$

The linear and nonlinear elastic stiffness matrices denoted by $[D],[D_1],[D_2],[D_3]$ can be expressed as

$$[D] = \int_{-\frac{h}{2}}^{+\frac{h}{2}} [L]^T [\bar{Q}][L] dz; [D_3] = \begin{bmatrix} A & 0 \\ 0 & A_1 \end{bmatrix}$$

$$[D_2] = \begin{bmatrix} A & B & E & 0 & 0 \\ 0 & 0 & 0 & A_1 & C_2 \end{bmatrix}; [D_1] = \begin{bmatrix} A & 0 \\ B & 0 \\ E & 0 \\ 0 & A_1 \\ 0 & C_1 \end{bmatrix}. \quad (11)$$

2.5 Work on external in-plane mechanical loading

The potential energy caused by the in-plane compressive uniform and non-uniform loading can be inferred from the work of Lal et al. [47] and Karamanli and Aydogdu [2].

$$\delta W = \int_A \frac{1}{2} W_x \left(\frac{\partial w}{\partial x} \right)^2 dA \quad (12)$$

where W_x is the in-plane compressive applied force, which can be expressed according to Karamanli and Aydogdu [2] as follows:

$$W_x = W \left[W_1 \left(x + \frac{a}{2} \right)^2 + W_2 \left(x + \frac{a}{2} \right) + W_3 \right]. \quad (13)$$

For uniform in-plane loading ($W_x = N_x^1$) condition, $W_1 = 0$, $W_2 = 0$, $W_3 = 1$.

For triangular in-plane loading ($W_x = N_x^2$) condition, $W_1 = 0$, $W_2 = 2$, $W_3 = 0$.

For triangular in-plane loading $(W_x = N_x^3)$ condition, $W_1 = 0$, $W_2 = -2$, $W_3 = 2$.

Similarly, the kinetic energy (*KE*) of the SMPFGMSC beam can be represented as

$$KE = \frac{1}{2} \int_0^l \int_{-h/2}^{+h/2} \rho(z) [W]^T [W] dz dx. \quad (14)$$

2.6 FEM formulation

For element (*e*), the displacement field vector (*p*) in terms of shape function (N_i) at the i^{th} node can be written as

$$\{p\}^e = \sum_{i=1}^{NN} [N_i]^T \{p_i\}^e; \quad \{x\}^e = \sum_{i=1}^{NN} [N_i]^T \{x_i\}^e \quad (15)$$

where the number of nodes per element are defined by *NN*, and *x* is the Cartesian coordinate. In summing the number of elements by FEM (Eq. (10)), the strain energy of the SMPFGMSC beam can be written as

$$S_T = \frac{1}{2} \sum_{i=1}^{NE} \left[\{p\}^{T(e)} \left(K_l + K_{nl} \right)^{(e)} \{p\}^{(e)} \right] \quad (16)$$

where K_l and $K_{nl} \left(= K_{nl_1} + K_{nl_2} + K_{nl_3} \right)$ are the linear and nonlinear stiffness matrices.

By using FEM in summing Eq. (12) for all numbers of an element, the loading can also be written as follows:

$$\delta W^{(e)} = \sum_{i=1}^{NE} \left\{ p^{(e)} \right\}^T W_x K_g^{(e)} \left\{ p^{(e)} \right\},$$

$$K_g^{(e)} = \frac{1}{2} \int_{A^{(e)}} G_n^{(e)T} W_x G_n^{(e)} dA. \quad (17)$$

The KE of the SMPFGMSC beam after summing the number of elements via FEM can be represented as

$$KE = \sum_{i=1}^{NE} \{p\}^{(e)T} [M]^{(e)} \{p\}^{(e)} dA \quad (18)$$

where [*M*] is the global consistent mass matrix. On the basis of Hamilton's principle, the equation of motion can be expressed as

$$\delta\pi = \int_{t_1}^{t_2} \left(\delta KE - \delta S_T + \delta W\right) dt = 0 . \quad (19)$$

Substituting Eqs. (10), (12) and (14) in Eq. (19) obtains

$$\left[M\right]\left\{\ddot{q}\right\} + \left[K - W_x K_g\right]\left\{p\right\} = \left[F_t\right]. \quad (20)$$

2.7 Instability analysis of SMPFGMSC beam

In the present study involving static analysis, dynamic analysis is also performed to evaluate the stability and instability boundaries. The periodic axial compressive force $W_x(t)$ is defined as

$$W_x(t) = W_s + W_d \cos\Omega t = \propto F_{cr} + \beta F_{cr} \cos\Omega t \quad (21)$$

where the excitation frequency or disturbing frequency is denoted by Ω; W_s and W_d are the static and dynamic load portions, respectively; $\alpha = \frac{w_s}{F_{cr}}$, $\beta = \frac{w_d}{F_{cr}}$, and F_{cr} are the percentages of the static buckling load called static and dynamic load factors and static buckling load.

Eq. (21) is integrated into Eq. (20). The dynamic instability equation further can be rewritten as

$$\left[M\right]\left\{\ddot{q}\right\} + \left[K - \left(\propto F_{cr} + \beta F_{cr} cos\Omega t\right) K_g\right]\left\{p\right\} = 0 . \quad (22)$$

Eq. (22) is a second-order DE with the Mathieu–Hill coefficient. From a practical viewpoint, knowing the boundaries of stability and instability regions (within periods of T and $2T$, $T = 2\pi / \omega$) is extremely important. The calculation is given by

$$\left[\left[K\right] - (\propto F_{cr}\left[K_g\right] \pm \frac{1}{2}\beta F_{cr}\left[K_g\right] - \left(\frac{\Omega}{\omega}\right)^2 \frac{\omega^2}{4}\left[M\right]\right]\left\{p\right\} = 0 \quad (23)$$

where the $(\pm)$ sign corresponds to the two extreme boundaries of the instability region, and Ω / ω represents the disturbing frequency for the input values of Ω and ω. The eigenvalues (Ω/ω) correspond to the disturbing frequency of the region of instability for the given values of α and β. For a given α value, the variation in Ω/ω with regard to β can be determined using standard eigenvalue algorithms. The plot of such variations in the β-(Ω/ω) plane represents the instability regions of the beam subject to the periodic axial load. The generalized equation of motion of Eq. (26) can be written as

$$\left[\left[K\right] - \left(\alpha \pm \frac{\beta}{2}\right) N_{cr}\left[K_g\right] - \left(\frac{\Omega}{\omega}\right)^2 \frac{\omega^2}{4}\left[M\right]\right]\left\{q\right\} = F . \quad (24)$$

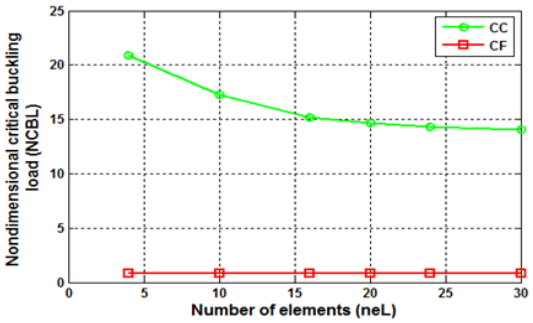

Fig. 2. Convergence study under different BCs.

3. Results and discussion

The static and dynamic instabilities of the SMPFGMSC and FGM beams were analyzed using HSDT with full nonlinearity via FEM in MATLAB. The dynamic instability region was evaluated using the Mathieu–Hill-type equation in Bolotin's method.

3.1 Convergence and validation study

The convergence study of the present finite element formulation was performed using various numbers of elements for the clamp-clamp and clamp-free BCs, in which the thickness ratio (a/h) was 20 and the ply orientation was $[90/0]_s$ (Fig. 2). As the number of elements increased, the non-dimensional critical buckling load (NCBL) began to converge. Hence, for the succeeding computation of the results, the number of elements was assumed to be 30.

The validation study of the NCBL of the structural composite under different BCs and in-plane buckling load is shown in Table 1. The findings indicate a close agreement of our result with those of Ozturk et al. [16] and Reddy [48] who used CLPT. Table 1 also shows the NCBL with the presently utilized HSDT model, which is in close congruence with the that of Karamanli and Karamanli [2] who performed HBT with the quasi-3D simulation method.

Tables 2 and 3 present the results of the validation study for the fundamental frequency parameters in combination with the results from Karaagac et al. [21], Loja et al. [19], and Ozturk et al. [16]. The results are in close agreement with the present analytic findings.

3.2 Analysis of FGM beam

Initially, for the dynamic analysis in the validation study, FGM beams with an Al rich bottom and a steel-rich bottom were considered. The length of the beam was 0.5 m, the width was 0.1 m, and the thickness was 0.25 m. The material properties were as follows:

Steel: $E_c = 210\times10^9$ Pa; $\upsilon_c = 0.3$; $\rho_c = 7850$ kg / m^3

Aluminum: $E_c = 70\times10^9$ Pa; $\upsilon_c = 0.3$; $\rho_c = 2707$ kg / m^3 .

Table 2. Comparison of fundamental frequency parameters: set 1.

Laminate	Present	Karaagac et al. [21]	Loja et al. [19]	Ozturk et al. [16]
0/90/0/90	9.55	9.50	8.760	9.45
0/30/-30/0	12.71	12.58	12.61	12.38
0/45/-45/0	12.47	12.333	12.40	12.08
0/60/-60/0	12.31	12.251	12.21	12.04

Table 3. Comparison of fundamental frequency parameters: set 2.

Present	Present	Karaagac et al. [21]
$[0_4]$	5.29	5.07
$[90_4]$	1.08	1.015
[0 90]s	4.92	4.77
[90 0]s	2.13	2.032

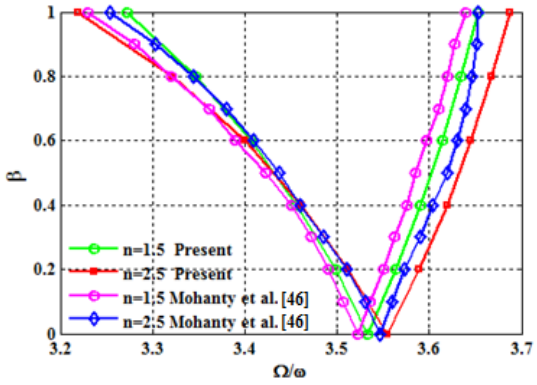

Fig. 3. Validation of dynamic instability regions versus dynamic in-plane load parameters for the FGM beam.

The fundamental frequency of an equivalent ordinary steel beam is ω = 6724.9, and the fundamental buckling load of an equivalent ordinary steel beam is P = 11.37×10^8 N. These values were used for stability analysis by Mohanty et al. [46]. In view of fully understanding the property variation and thickness with respect to n, the effect of amplitude ratio and temperature variation on dynamic stability were determined (Figs. A.1-A.3 in the Appendix).

Fig. 3 shows a validation of the dynamic instability regions versus the dynamic in-plane load parameters for the supported FGM beam only. As the power law index (n) increased, the dynamic instability became apparent at the higher disturbing frequency, and the width of the instability regions also increased. The present numerical results based on the HSDT with C^0 FEM analysis for the different volume fraction exponents (n) are in good agreement with the results of Mohanty et al. [46] who used FSDT with an analytical approach.

Fig. 4 depicts the difference in the dynamic instability region between (a) the layered composite and sandwich composite (0/C/0) (set 1) and (b) the single-layer FGM and three-layered sandwich FGM composite (0/F/0) with the supported beam only (set 2) and amplitude ratio of W_{max}/h = 0.1. The sandwich

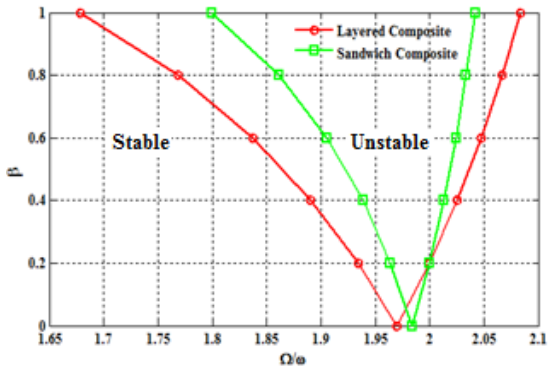

(a)

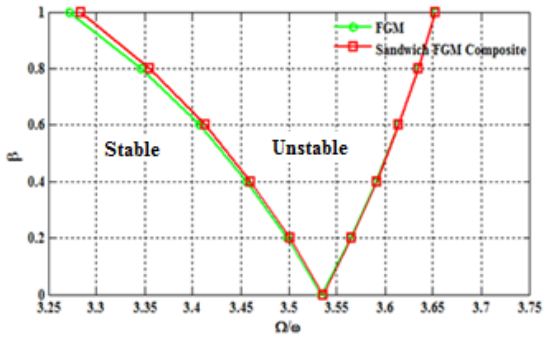

(b)

Fig. 4. Variation of the dynamic instability region for the FGM, sandwich, and layered composite beams.

structure core to the sheet thickness was taken as $t_c / t_f = 20$.

The comparison revealed that the stability region extended under the sandwich composite (0/C/0) and sandwich FGM composite (0/F/0) beams. Although the FGM considerably benefitted from the composite materials, the sandwich FGM composite beam also gained from the setup. Thus, in micro-electromechanical system (MEMS), nano-electromechanical system (NEMS), defense, maritime, automotive, and space applications, the sandwich FGM composite can be utilized on the basis of the inferred results.

Core properties (C): $m_{1c} = 5,\quad m_{2c} = 0.6,\quad m_{3c} = 0.25,$
$E_{2c} = 10.3e^3$ Pa, $\upsilon_{12c} = 0.25,\quad E_{1c} = m_{1c} * E_{2c},$
$G_{12c} = m_{2c} * E_{2c},\quad G_{13c} = G_{12c},\quad G_{23c} = m_{3c} * E_{2c},$
$\upsilon_{21c} = \upsilon_{12c}\left(\frac{E_{2c}}{E_{1c}}\right),\quad \rho_C = 1.$

Set 1 (S1): $E_1 = 170e^9$ Pa, $E_2 = 9.5e^9$ Pa,
$G_{12} = 5.1565e^9$ Pa, $\upsilon_{12} = 0.3,\quad \rho = 1550.06,$
$G_{23} = 2.5414e^9$ Pa, $G_{13} = 4.3053e^9$ Pa, $\upsilon_{21} = \upsilon_{12c}\left(\frac{E_2}{E_1}\right).$

Set 2 (S2): $E_1 = 155e^9$ Pa, $E_2 = 9.5e^9$ Pa,
$G_{12} = 5.1565e^9$ Pa, $\upsilon_{12} = 0.3,\quad \rho = 1550.06,$
$G_{23} = 2.5414e^9$ Pa, $G_{13} = 4.3053e^9$ Pa, $\upsilon_{21} = \upsilon_{12c}\left(\frac{E_2}{E_1}\right).$

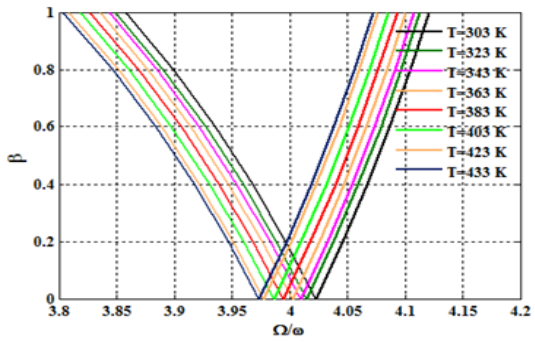

Fig. 5. Effect of temperature on TD sandwich FGM composite beam.

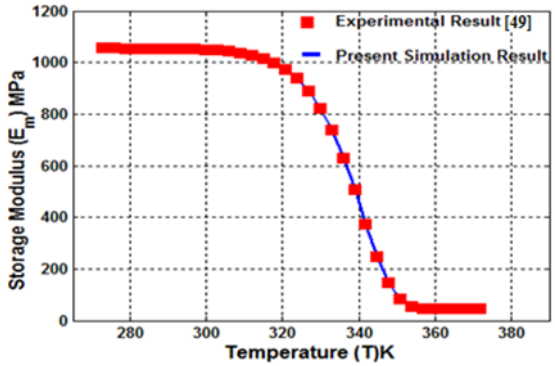

Fig. 6. Influence of dynamic temperature variation on the elastic modulus of SMP.

Set 3 (S3): $m_1 = 1,\quad m_2 = 0.5,\quad m_3 = 0.2,\quad E_2 = 10.3e^3$ Pa, $\upsilon_{12} = 0.25,\quad E_1 = m_1 * E_2,\quad G_{12} = m_2 * E_2,\quad G_{13} = G_{12},$ $G_{23} = m_3 * E_{2c},\quad \upsilon_{21} = \upsilon_{12}\left(\frac{E_2}{E_1}\right),\quad \rho = 1.$

3.3 Analysis of SMP sandwich FGM composite beam

Fig. 5 shows the effect of temperature on the TD property of the sandwich FGM composite (0/F/0) for the supported beam only under full nonlinearity (W_{max}/h = 0.08) with S1 and α = 0.1. The analysis of the facesheet and bottom sheet are for the SMPC, whereas the core is for the FGM. In the analysis, the temperature varies from 303 to 433 K. The range encompasses the glass transition temperature (T_g) of the matrix, and its effect is plotted. As the temperature increased, the values shift towards the lower-excitation frequency.

Fig. 6 shows the effect of dynamic temperature variation on the elastic modulus of SMP in the temperature range from 273 to 373 K across T_g. The findings are compared with the experimental result of Kumpfer and Rowan [49]. The parameters considered in this work have been discussed in Sec. 2. The loss modulus is negligible with respect to the storage modulus. Thus, in this study, the storage modulus is considered to be the Young's modulus, similar to the work of Gu et al. [42].

The effect of the dynamic temperature variation on the CBL of the sandwich FGM composite beam is shown in Fig. 7. The

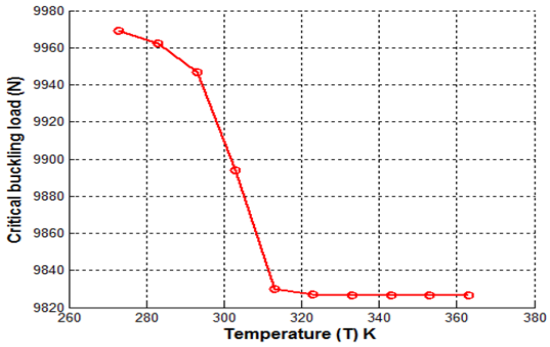

Fig. 7. Effect of dynamic temperature variation on CBL.

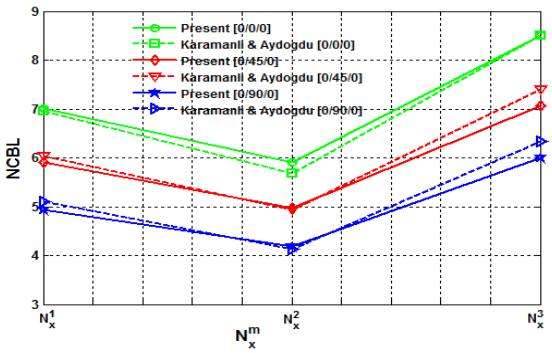

Fig. 8. Variation in dimensionless CBL under different VILs.

following values are considered: amplitude ratio of 0.1, n = 1.5, V_f = 10 %, core-to-sheet thickness ratio of 10. The simply supported BC only is analyzed at varying temperatures from 273 to 363 *K*. Temperature plays an important role in the structural and mechanical properties of SMPC and SMPFGMSC. The dynamic performance of the polymer and the corresponding composites in glass transition region is shown in Fig. 7. The result highlights the influence of the glass transition region of the SMP matrix on the CBL of SMPC laminates, as depicted by the abruptly declining curve in the region. These inferences can be substituted in the subsequent phases of FEM to comprehend the dynamic behavior of the SMPFGMSC beam with respect to temperature.

3.4 Analysis of composite beam under VIL

The validation results from using different VILs are presented in Fig. 8. The results specified in the work of Karamanli and Karamanli [2] are considered in the assessment.

An evaluation of the NCBL is performed for the CC BC depicting a symmetric ply-oriented composite beam. The assessment depicts a close agreement of the present analytical results with the previously published results.

The effects of β-transition temperature (T_β) and T_g with α = 0.1 under VIL conditions on the dynamic stability of SMPFGMSC beam are determined for the first time, as shown in Figs. 9(a) and (b), respectively. The unstable region of N_x^3 is lower than those of N_x^1, and N_x^2, and N_x^1 has a secure

Table 4. Effect of VIL on different types of composites under different temperature conditions.

Temp. (T)	Type of composite	N_x^1 (N)	N_x^2 (N)	N_x^3 (N)
---	Layered	1.05×10^6	8.61×10^5	1.36×10^6
	Layered FGM	7.72×10^6	6.30×10^6	9.96×10^6
T_β	SMPC	2.04×10^6	1.66×10^6	2.63×10^6
	SMPFGMSC	8.28×10^6	6.76×10^6	1.07×10^7
T_g	SMPC	2.04×10^6	1.62×10^6	2.63×10^6
	SMPFGMSC	8.28×10^6	6.75×10^6	1.07×10^7

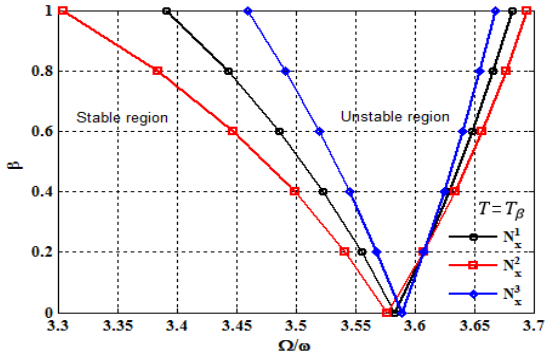

(a)

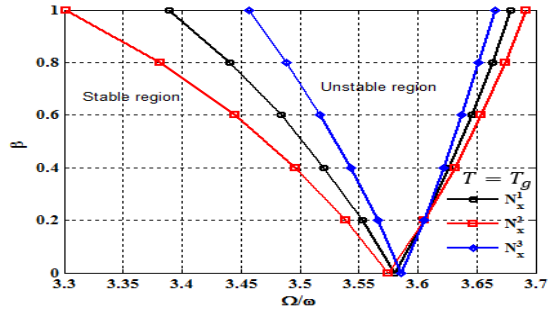

(b)

Fig. 9. Effect of VIL on dynamic stability of the SMPFGMSC beam.

intermediate unstable region with respect to those of N_x^3 and N_x^2.

The results of the stability and instability analyses of the layered FGM and SMPFGMSC beam are shown in Fig. 10. Under VIL (N_x^1 , N_x^2 , N_x^3) conditions, the unstable region of the SMPFGMSC compared is lower than that of the layered FGM. The comparison between the layered composites, FGM sandwich composites, SMPC, and SMPFGMSC beams are presented in Table 4. The SS BC, thickness ratio of 10, amplitude ratio of 0.1, β-transition temperature (T_β), and flow region temperature (T_f) are considered. The buckling resistance of the layered FGM and SMPC improved by 86 % and 48 % with respect to the layered composites, respectively. Although the layered FGM is more suitable than the SMPC and layered composite, the buckling resistance is 7 % higher for the SMPFGMSC beam at T_β .

The effect of the dynamic temperature variation, BCs, fiber

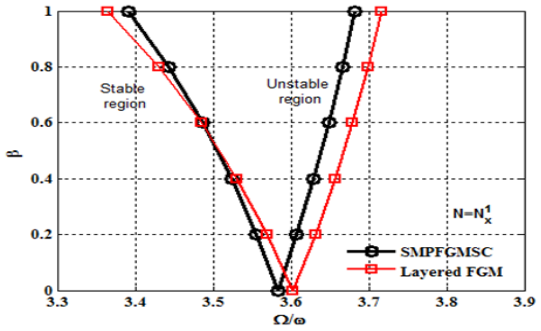

(a)

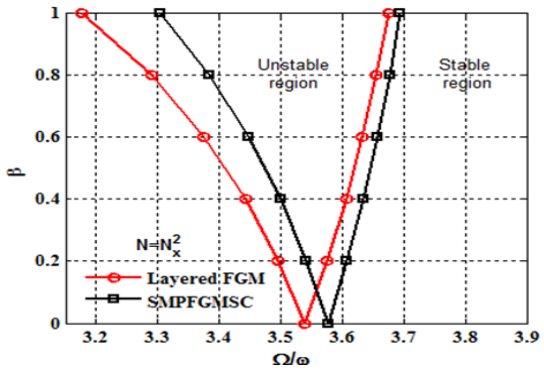

(b)

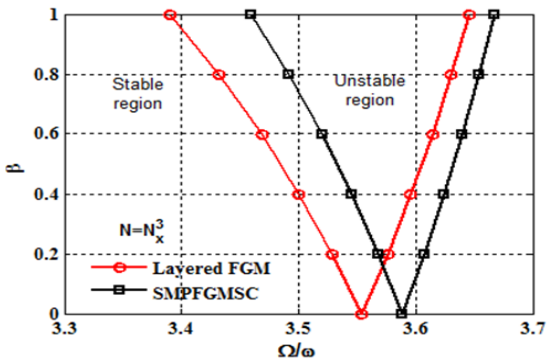

(c)

Fig. 10. Instability analysis in layered FGM and SMPFGMSC beam under: (a) N_x^1 ; (b) N_x^2 ; (c) N_x^3 .

variation, and beat displacement response on the SMPFGMSC can be inferred from Figs. A.4-A.10 in the Appendix.

4. Conclusions

The well-established HSDT, in conjunction with the nonlinear von Karman kinematics, was computed in the present study. Post-buckling, static, and dynamic analyses under uniform and non-uniform in-plane axial compressive periodic loading conditions were performed for the first time to explore the combined effect of the SMPC facesheet and bottom sheet and the FGM core. Then, a convergence study was performed to select a number of elements. The validation study verified the compatibility and accuracy of the presently utilized analytical HSDT

model based on the comparison of results obtained from the reviewed literature. On the basis of the study, the following observations are presented:

a) For the FGM beam, the nonlinear dynamic analysis shows that as the temperature increased from 300 to 350 K, the instability region shifts towards the lower disturbing frequency. The stability region is extended for the sandwich composite (0/C/0) and sandwich FGM composite (0/F/0) beams with respect to the layered composite and FGM beams, respectively. Thus, the sandwich FGM composite can find its applications in the MEMS, NEMS, and space fields based on the inferred results in this study.

b) The effect of the β-transition temperature (T_β) and glass transition temperature (T_g) under VIL conditions on the dynamic stability of the SMPFGMSC beam has been presented for the first time in this study. The unstable region for N_x^3 is lower than those of N_x^2 and N_x^1. The intermediate unstable region is obtained for N_x^3 and N_x^2.

c) Under VIL (N_x^1, N_x^2, N_x^3) conditions, the unstable region of the SMPFGMSC is lower than that of the layered FGM.

References

[1] N. D. Duc, Nonlinear dynamic response of imperfect eccentrically stiffened FGM double curved shallow shells on elastic foundation, *J. Composite Structures*, 99 (2013) 88-96.

[2] A. Karamanli and M. Aydogdu, Buckling of laminated composite and sandwich beams due to axially varying in-plane loads, *Composite Structures,* 210 (2019) 391-408.

[3] R. K. Gupta, J. B. Gunda, G. R. Janardhan and G. V. Rao, Post-buckling analysis of composite beams: simple and accurate closed-form expressions, *Composite Structures*, 92 (8) (2010) 1947-1956.

[4] S. D. Akbas, Hygrothermal post-buckling analysis of laminated composite beams, *International Journal of Applied Mechanics*, 11 (1) (2019) 1950009.

[5] S. J. Song and A. M. Waas, Effects of shear deformation on buckling and free vibration of laminated composite beams, *Composite Structures*, 37 (1) (1997) 3343.

[6] J. Lee, S. E. Kim and K. Hong, Lateral buckling of i-section composite beams, *Engineering Structures*, 24 (7) (2002) 955964.

[7] S. K. Singh and A. Chakrabarti, Buckling analysis of laminated composite plates using an efficient C0 FE model, *A. Lat. Am. J. Solids Struct*., 9 (3) (2012) 1-13.

[8] M. K. Ranganatha Swamy, U. S. Mallikarjun and V. Udayakumar, Synthesis and characterization of shape memory polymers, *IOP MSE*, 577 (2019) 012095.

[9] D. W. Hanzon, K. Yu and C. M. Yakacki, Chapter 5 - active mechanisms of shape-memory polymers, *Shape-Memory Polymer Device Design*, William Andrew Publishing (2017) 139-187.

[10] D. M. Feldkamp and I. A. Rousseau, Effect of the deformation temperature on the shape-memory behavior of epoxy networks, *Macromolecular Materials and Engineering*, 295 (8) (2010) 726-734.

[11] J. Leng, L. Xin, Y. Liu and S. Du, Shape-memory polymers and their composites: stimulus methods and applications, *Progress in Materials Science*, 56 (7) (2011) 1077-1135.

[12] C. S. Zhang and Q. Q. Ni, Bending behavior of shape memory polymer based laminates, *Composite Structures*, 78 (2) (2007) 153-161.

[13] A. Lal and K. Markad, Influence of dynamic temperature variation and inplane varying loads over post-buckling and free vibration analysis of sandwich composite beam, *International Journal of Computational Materials Science and Engineering,* 9 (3) (2020) 2050012.

[14] G. A. Zizicas, Dynamic buckling of thin plates, *Trans. ASME,* 74 (7) (1952) 1257-1268.

[15] L. Librescu and N. K. Chandiramani, Dynamic stability of transversely isotropic viscoelastic plates, *Journal of Sound and Vibration*, 130 (3) (1989) 467-486.

[16] H. Ozturk and M. Sabuncu, Stability analysis of a cantilever composite beam on elastic supports, *Composites Science and Technology*, 65 (2005) 1982-1995.

[17] M. Touratier, An efficient standard plate theory, *International Journal of Engineering Science*, 29 (1991) 901-916.

[18] A. Beakou and M. Touratier, A rectangular plate finite element for analysing composite multilayered shallow shell in statics, vibration and buckling, *International Journal for Numerical Methods in Engineering*, 36 (1993) 627-653.

[19] M. A. R. Loja, J. I. Barbosa and C. M. M. Soares, Static and dynamic behaviour of laminated composite beams, *International Journal of Structural Stability and Dynamics*, 1 (4) (2001) 545-560.

[20] G. K. Binnur, Static and dynamic stability analyses of the symmetric laminated cantilever beams, *Advanced Composites Letters*, 17 (5) (2008).

[21] C. Karaagac, H. Ozturk and M. Sabuncu, Lateral dynamic stability analysis of a cantilever laminated composite beam with an elastic support, *International Journal of Structural Stability and Dynamics*, 7 (3) (2007) 377-402.

[22] N. V. Thanh, N. D. Khoa, N. D. Tuan, P. Tran and N. D. Duc, Nonlinear dynamic response and vibration of functionally graded carbon nanotubes reinforced composite (FG-CNTRC) shear deformable plates with temperature dependence material properties and surrounded on elastic foundations, *J. Thermal Stresses*, 40-10 (2017) 1254-1274.

[23] Y. Fu, J. Wang and Y. Mao, Nonlinear analysis of buckling, free vibration and dynamic stability for the piezoelectric functionally graded beams in thermal environment, *Appl. Math. Model*., 36 (9) (2012) 4324-4340.

[24] N. D. Duc, T. Q. Quan and V. D. Luat, Nonlinear dynamic analysis and vibration of shear deformable piezoelectric FGMdouble curved shallow shells under damping-thermo-electro-mechanical loads, *J. Composite Structures*, 125 (2015) 29-40.

[25] H. S. Shen, Thermal postbuckling behavior of shear deformable FGM plates with temperature-dependent properties, *Int. J. Mech. Sci*., 49 (4) (2007) 466-478.

[26] H. S. Shen, Postbuckling of FGM plates with piezoelectric actuators under thermo-electro-mechanical loadings, *Int. J. Solids Struct.*, 42 (23) (2005) 6101-6121.
[27] F. A. Fazzolari, Stability analysis of FGM sandwich plates by using variable-kinematics Ritz models, *Mechanics of Advanced Materials and Structures*, 23 (9) (2016) 1104-1113.
[28] M. Zamanzadeh, G. Rezazadeh, I. Jafarsadeghipoornaki and R. Shabani, Static and dynamic stability modeling of a capacitive FGM micro-beam in presence of temperature changes, *Applied Mathematical Modelling*, 37 (10-11) (2013) 6964-6978.
[29] L. C. Trinh, T. P. Vo, H. T. Thai and T. K. Nguyen, Size dependent vibration of bi-directional functionally graded microbeams with arbitrary boundary conditions, *Composites Part B: Engineering*, 134 (2018) 225-245.
[30] N. D. Duc, Nonlinear thermo-electro-mechanical dynamic response of shear deformable piezoelectric sigmoid functionally graded sandwich circular cylindrical shells on elastic foundations, *Journal of Sandwich Structures and Materials,* 20 (3) (2016) 351-378.
[31] N. D. Duc, *Nonlinear Static and Dynamic Stability of Functionally Graded Plates and Shells*, Vietnam National University Press, Hanoi (2014).
[32] N. V. Thanh, V. D. Quang, N. D. Khoa, S. E. Kim and N. D. Duc, Nonlinear dynamic response and vibration of FG CNTRC shear deformable circular cylindrical shell with temperature dependent material properties and surrounded on elastic foundations, *Journal of Sandwich Structures and Materials,* 21 (7) (2018) 2456-2483.
[33] N. D. Duc and P. D. Nguyen, The dynamic response and vibration of functionally graded carbon nanotubes reinforced composite (FG-CNTRC) truncated conical shells resting on elastic foundation, *Materials*, 10 (2017) 1194.
[34] P. H. Cong, N. D. Khanh, N. D. Khoa and N. D. Duc, New approach to investigate nonlinear dynamic response of sandwich auxetic double curves shallow shells using TSDT, *Composite Structures*, 185 (2018) 455-465.
[35] N. D. Duc, T. Q. Quan and N. D. Khoa, New approach to investigate nonlinear dynamic response and vibration of imperfect functionally graded carbon nanotube reinforced composite double curved shallow shells subjected to blast load and temperature, *Journal Aerospace Science and Technology*, 71 (2017) 360-372.
[36] T. Q. Quan and N. D. Duc, Nonlinear thermal stability of eccentrically stiffened FGM double curved shallow shells, *J. Thermal Stresses*, 40 (2) (2016) 211-236.
[37] N. D. Duc, S. E. Kim, P. H. Cong, N. T. Anh and N. D. Khoa, Dynamic response and vibration of composite double curved shallow shells with negative poisson's ratio in auxetic honeycombs core layer on elastic foundations subjected to blast and damping loads, *International Journal of Mechanical Sciences*, 133 (2017) 504-512.
[38] V. T. T. Anh and N. D. Duc, Nonlinear response of shear deformable S-FGM shallow spherical shell with ceramic-metal-ceramic layers resting on elastic foundation in thermal environment, *J. Mechanics of Advanced Materials and Structures*, 23 (8) (2015) 926-934.
[39] N. D. Duc and T. Q. Quan, Nonlinear dynamic analysis of imperfect FGM double curved thin shallow shells with temperature-dependent properties on elastic foundation, *Journal of Vibration and Control,* 21 (7) (2013) 1340-1362.
[40] K. K. Westbrook, P. H. Kao, F. Castro, Y. Ding and H. J. Qi, A 3D finite deformation constitutive model for amorphous shape memory polymers: a multi-branch modeling approach for non-equilibrium relaxation processes, *Mechanics of Materials*, 43 (2011) 853-869.
[41] J. Gu, J. Leng and H. Sun, A constitutive model for amorphous shape memory polymers based on thermodynamics with internal state variables, *Mechanics of Materials*, 111 (2017) 1-14.
[42] J. Gu, J. Leng, H. Sun, H. Zeng and Z. Cai, Thermomechanical constitutive modeling of fiber reinforced shape memory polymer composites based on thermodynamics with internal state variables, *Mechanics of Materials*, 130 (2019) 9-19.
[43] C. A. Mahieux and K. L. Reifsnider, Property modeling across transition temperatures in polymers: a robust stiffness-temperature model, *Polymer*, 42 (7) (2001) 3281-3291.
[44] H. J. Qi, T. D. Nguyen, F. Castro, C. M. Yakacki and R. Shandas, Finite deformation thermo-mechanical behavior of thermally induced shape memory polymers, *Journal of the Mechanics and Physics of Solids*, 56 (5) (2008) 1730-1751.
[45] P. R. Heyliger and J. N. Reddy, A higher order beam finite element for bending and vibration problems, *J. Sound Vib.,* 126 (2) (1988) 309-326.
[46] S. C. Mohanty, R. R. Dash and T. Rout, Static and dynamic stability analysis of a functionally graded Timoshenko beam, *International Journal of Structural Stability and Dynamics*, 12 (4) (2012) 1250025.
[47] A. Lal, N. M. Kulkarni and B. N. Singh, Stochastic thermal post buckling response of elastically supported laminated piezoelectric composite plate using micromechanical approach, *Curv. Layer. Struct.,* 2 (2015) 331-350.
[48] J. N. Reddy, *Mechanics of Laminated Composite Plates Theory and Analysis*, CRS Press, New York (1997).
[49] J. R. Kumpfer and S. J. Rowan, Thermo-, photo-, and chemo-responsive shape-memory properties from photo-cross-linked metallo-supramolecular polymers, *J. Am. Chem. Soc.*, 133 (2011) 12866-12874.

Appendix

A.1 Analysis of FGM beam

Using the considered material property and power-law distribution equation, the variation that occurred into the effective material property in FGM through-thickness is shown in Fig. A.1. The figure indicates the nature of variation of elastic modulus, Poisson's ratio and density with power-law index (n_i, i = 0, 0.5, 1, 2, 5, 10).

Fig. A.2 shows the effect of nonlinearity (W_{max}/h = 0, 0.1, 0.15, 0.2) on the instability region of FGM beams for volume fraction exponents n = 1.5 and a/h = 2 under simply supported

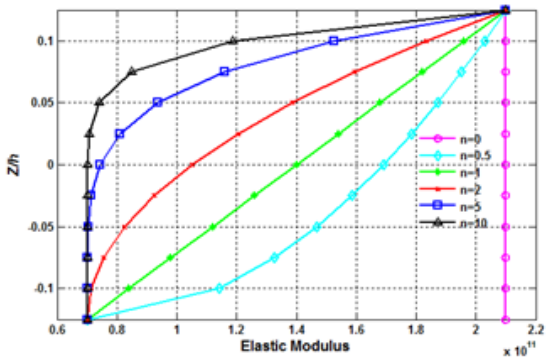

(a)

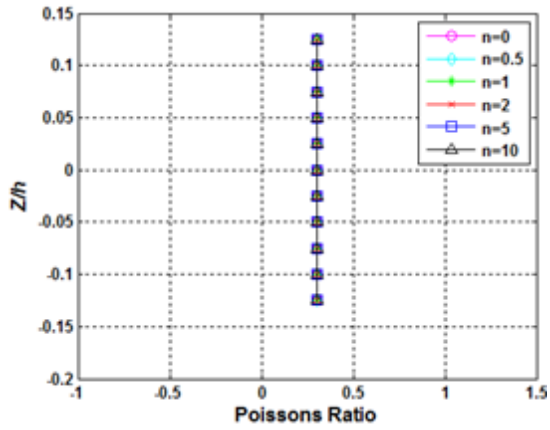

(b)

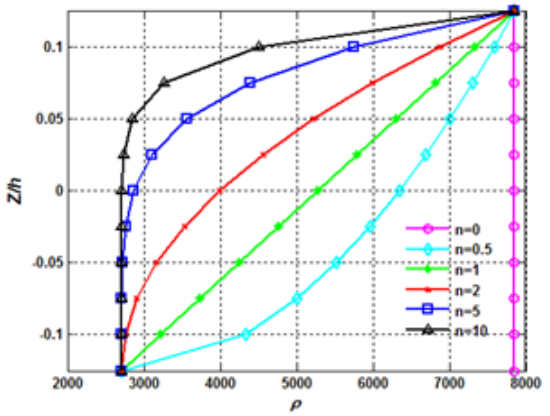

(c)

Fig. A.1. Variation of (a) elastic modulus; (b) Poissons ratio; (c) density along thickness as per '*n*'.

boundary condition. It is observed that the instability region shifts to higher disturbing frequency and the instability region becomes narrow as the linear model changes to the nonlinear model.

Temperature dependent material property is one of the interesting factors in the study. During the study, volume fraction exponents n = 1.5, a/h = 2, W_{max}/h = 0.2 with temperature dependent FGM beam was used and properties referred from Fu et al. [23], and the variation in nonlinear dynamic instability

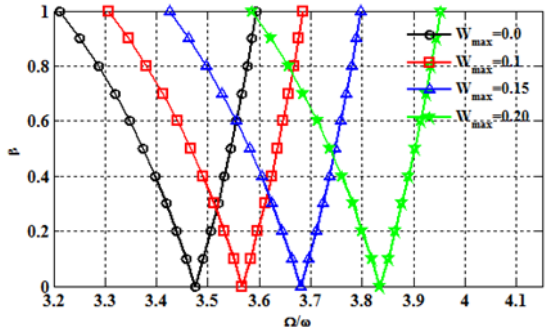

Fig. A.2. Effect of amplitude ratio over dynamic instability region.

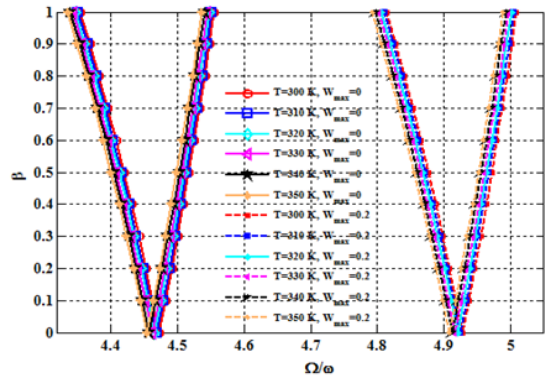

Fig. A.3. Variation in dynamic instability region with temperature.

region with temperature is shown in Fig. A.3. Results show that with the increase of temperature from 300 *K* to 350 *K*, the instability region shifted towards a lower disturbing frequency. With the elevation of temperature, the stiffness of the beam is reduced which affects the instability region.

A.2 Analysis of SMP sandwich FGM composite beam

The properties of composite material were estimated through the theory of volume averaging, as per the assumption that new two phase matrix and fiber have similar deformations (Gu et al. [42]). To evaluate the corresponding material properties of composites, Eqs. (14)-(18) were utilized. Fig. A.4 indicates the (a) longitudinal modulus, (b) transverse modulus, (c) shear modulus and (d) Poissons ratio of shape memory polymer composite (SMPC). Material properties varied drastically due to the dynamic property in the glass transition region of the SMP matrix. Prior to the glass transition region, SMPC act as an elastic material with longitudinal modulus of 2.395 GPa whereas after the region it again act as elastic with modulus of 2.3 MPa, as shown in Fig. A.4(a). Reduction of 4.13% was noticed in the longitudinal modulus of SMPC in the glass transition region. Similarly, the approximate reduction of 84% and 11% was observed in transverse and shear modulus of SMPC respectively as described in Figs. A.4(b)-(d).

Fig. A.5 represents effect of static load factor and amplitude ratio over SMP sandwich FGM composite beam at 303 K, n =

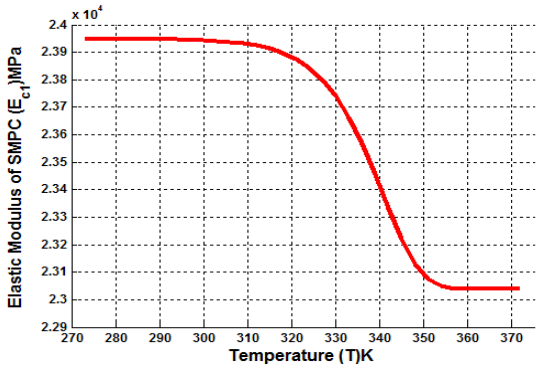

(a)

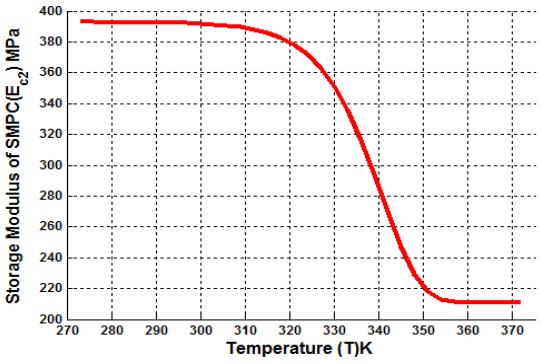

(b)

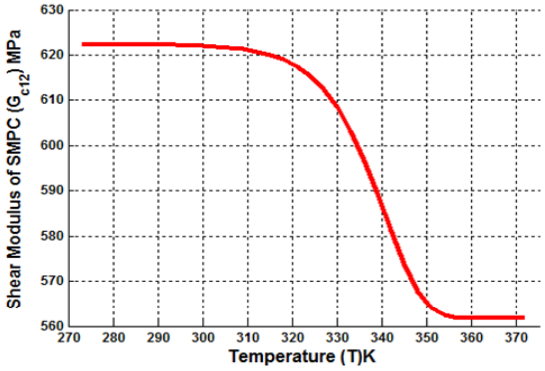

(c)

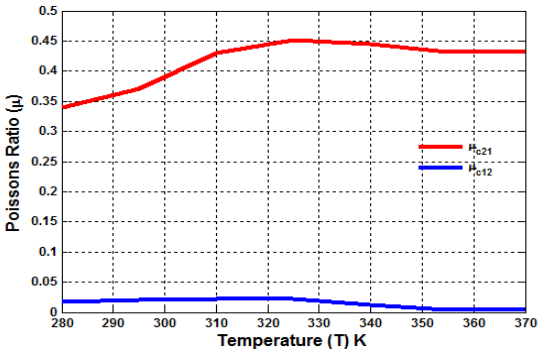

(d)

Fig. A.4. Effect of temperature variation over (a) longitudinal modulus E_{c1}; (b) transverse modulus E_{c2}; (c) shear modulus G_{c12}; (d) Poisson's ratio of SMPC.

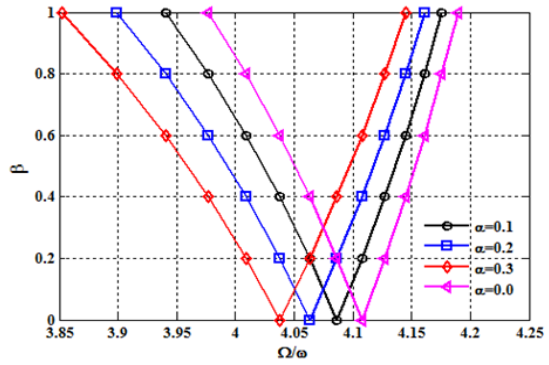

(a)

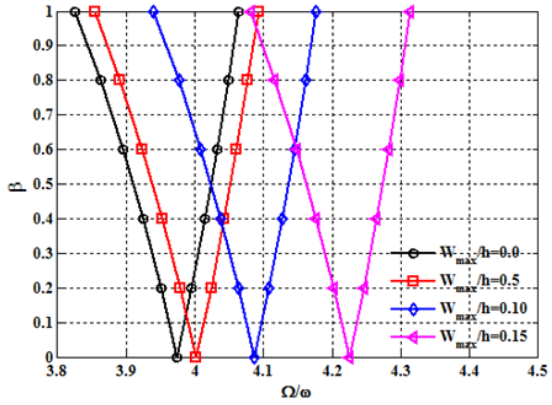

(b)

Fig. A.5. Effect of (a) static load factor; (b) amplitude ratio over SMP sandwich FGM composite beam.

1.5, (0/F/0) under simply supported BC. Fig. A.5(a) shows the effect of dynamic load portion with and without static load portion in inplane load. With the addition of the static load factor dynamic insatiability into the structure arises whereas it is minimal without static load factor. Fig. A.5(b) shows that instability region at α = 0.1, which moves to higher disturbing frequency and the instability region becomes contracted as the linear model changes to the nonlinear model.

Fig. A.6 shows the effect of thickness ratio variation on critical buckling load (CBL) under simply supported BC, W_{max}/h = 0.5, n = 1.5, core to sheet thickness ratio of 10 at $T = T_B$, $T = T_g$, and $T = T_f$ over [0/F/0] SMPFGMSC beam. As observed in Fig. 7 with increasing temperature, the resistance against buckling gets reduced down in the vicinity of T_g. A magnified view of the reduction in CBL concerning beam thickness ratio at β-transition temperature (T_β), glass transition temperature (T_g) and flow region temperature (T_f) is shown in Fig. A.6. This is particularly happening because of nature of the beam varied from thick to thin region. Fig. A.6 also depict the more buckling resistance offered in β-transition temperature region (T_β) than temperature at the beginning of the flow region (T_f). The reasons is material properties varied drastically due to the dynamic property in the glass transition region periphery of the SMP matrix as shown in Fig. A.4.

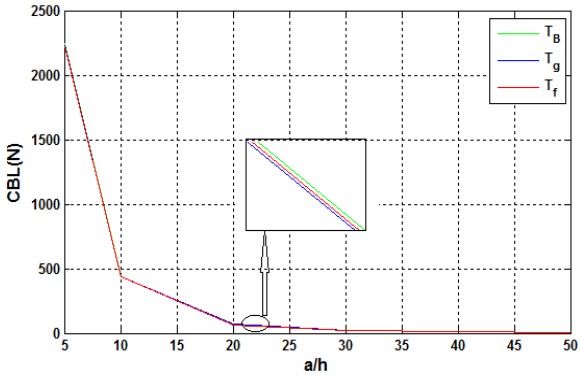

Fig. A.6. Variation in CBL with beam thickness ratio across glass transition region.

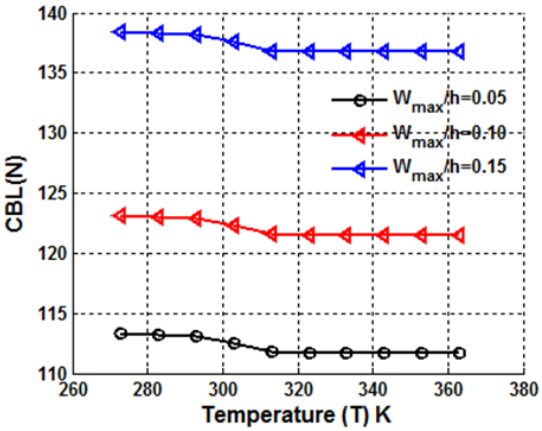

(a) Simply supported BC

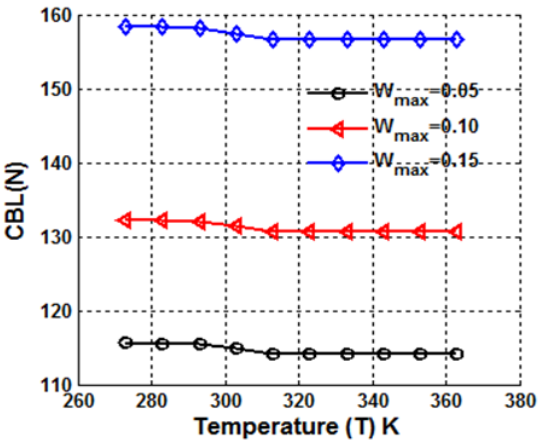

(b) Clamped-free BC

Fig. A.7. Effect of dynamic temperature and amplitude ratio variation over SMPFGMSC under (a) SS; (b) CF boundary conditions.

Effect of dynamic temperature variation over SMPFGMSC (0/F/0) beam in terms of CBL under (a) simply supported and (b) clamped free BC under uniform in-plane load is shown in Fig. A.7. The figure clearly shows that, as the linear model varied to the nonlinear model, CBL increased by 8% and 12% during the comparison between two successive amplitude ratios. Similarly, the rise of 14% and 20 % was noticed in CBL for the case of clamped free (CF) BC for two successive amplitude ratios.

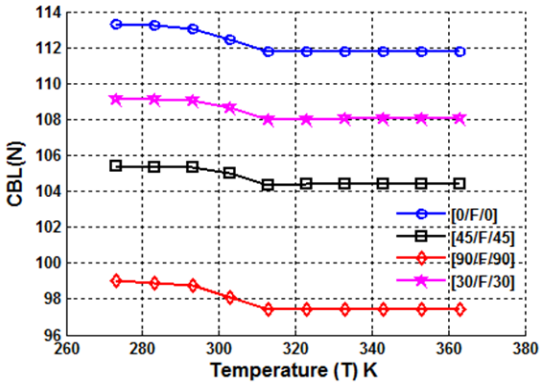

Fig. A.8. Effect of fiber orientations over CBL under dynamic temperature variation.

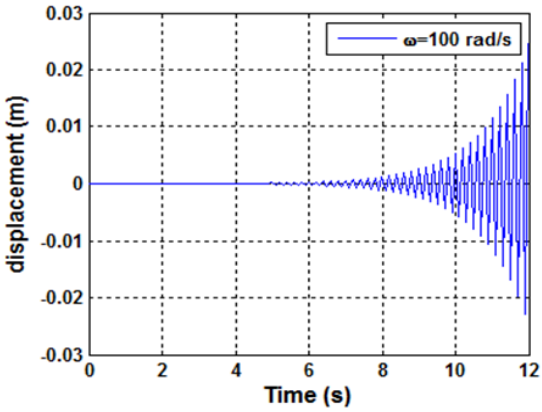

(a) 0/F/0

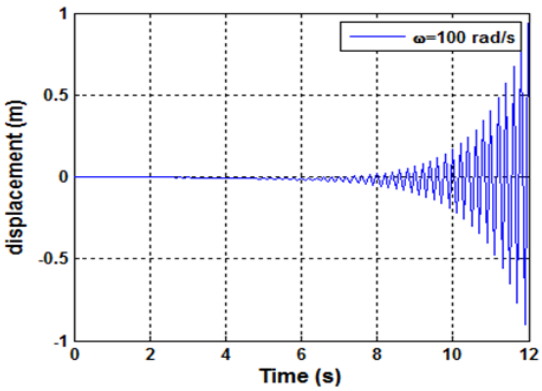

(b) 0/C/0

Fig. A.9. Beat displacement response of (a) SMPFGMSC; (b) SMPSC beam.

Fig. A.8 shows the effect of fiber layup variation in facesheet and bottom sheet of SMPFGMSC under dynamic temperature variation in the vicinity of glass transition temperature and simply supported (SS) BC, with W_{max}/h = 0.05, a/h = 10. Results clearly reveal that when fibers were oriented in longitudinal

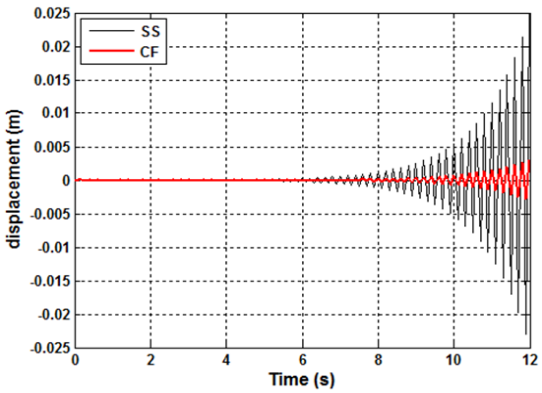

Fig. A.10. Effect of boundary conditions over displacement response of SMPFGMSC beam.

directions, it provides 4%, 4% and 6% more buckling resistance than 30^0, 45^0 and 90^0 fiber orientation, respectively.

The visualization of beat displacement response of the SMPFGMSC and shape memory polymer sandwich composite (SMPSC) beam under simply supported BC with 100 rad/sec is differentiated in Figs. A.9(a) and (b). Under inplane loading in unstable region, the displacement response of the SMPFGMSC and SMPSC beam was examined and concluded that as compared to SMPSC, minimal displacement was observed in case of SMPFGMSC beam. For the present analysis, set S1 properties were selected for the sheet of SMPSC whereas core properties were utilized for sheet of SMPFGMSC. The displacement response shows an increasing order due to the compressive periodic in-plane load under higher dynamic loading factor. It is hazardous, unpredictable and may cause failure of the structures, while carrying dynamic load parameter, and this presents the opportunities to the researchers and engineers to remove the instability existing in the model/structures with control of loadings, nonlinearity and damping of member. Similarly, Fig. A.10 shows the effect of BC over beat displacement response of SMPFGMSC beam considering t_c/t_f = 10, and beam thickness ratio of 10. As compared to SS BC, lesser beat displacement response was obtained with the CF BC.

Kanif M. Markad was born in Ahmednagar, Maharashtra, India, in 1987. He received Bachelor's degree in Mechanical Engineering from Pune University, Master's degree in Design Engineering from Solapur University and presently working as a Research Scholar in Mechanical Engineering Department, SVNIT, Surat, India. His main research interest includes numerical analysis of composite materials, smart materials, manufacturing and analysis of smart hybrid materials.